Surfaces and Interfaces 98 (2026) 110387

Contents lists available at ScienceDirect

Surfaces and Interfaces

journal homepage: www.sciencedirect.com/journal/surfaces-and-interfaces

Comparative kinetics of CuAAC and thiol–yne click chemistries for high-density streptavidin immobilization on alkyne-terminated glass surfaces

Seyed Mohammad Mahdi Dadfar [a,b,*], Sylwia Sekula-Neuner [c], Vanessa Trouillet [d], Yvonne Joseph [b], Michael Hirtz [a,*]

[a] Institute of Nanotechnology (INT) & Karlsruhe Nano Micro Facility (KNMFi), Karlsruhe Institute of Technology (KIT), Kaiserstraße 12, 76131 Karlsruhe, Germany
[b] Institute of Nanoscale and Biobased Materials, Faculty of Materials Science and Technology, TU Bergakademie Freiberg, Gustav-Zeuner-Str. 3 09599 Freiberg, Germany
[c] n.able GmbH, Hermann-von-Helmholtz-Platz 1, 76344 Eggenstein-Leopoldshafen, Germany
[d] Institute for Applied Materials (IAM) & Karlsruhe Nano Micro Facility (KNMFi) Karlsruhe Institute of Technology (KIT) Hermann-von-Helmholtz-Platz 1 76344 Eggenstein-Leopoldshafen, Germany

ARTICLE INFO

Keywords:
Click chemistry
Surface functionalization
CuAAC
Thiol–yne coupling
Streptavidin immobilization

ABSTRACT

This study presents a systematic comparison of two prominent click chemistries, copper-catalyzed azide–alkyne cycloaddition (CuAAC) and thiol-yne coupling (TYC), for the controlled immobilization of biological macromolecules on glass surfaces. Two distinct alkyne-terminated surfaces were fabricated: a short-chain 4-pentynoic acid surface and a long-chain polyethylene glycol (PEG) surface prepared with Alkyne PEG Silane (ALK-PEG-Si, MW 3400). The efficiency of biotin immobilization, followed by subsequent binding of the protein streptavidin, was evaluated kinetically over 10, 20, and 40 min. The results indicate that the choice of surface chemistry profoundly influences reaction kinetics. CuAAC proceeded most efficiently on the flexible, hydrophilic ALK-PEG-Si surface, achieving high streptavidin binding density at 20 min. In contrast, TYC demonstrated a faster initial reaction rate on the rigid, hydrophobic 4-pentynoic acid surface, reaching near-maximal intensity within 10 min. At longer reaction times (40 min), both chemistries and both surfaces converged to similar maximum immobilization levels. This work provides a fundamental understanding of how the interplay between linker design and click reaction mechanism can be strategically exploited to optimize the kinetics and density of macromolecular immobilization for applications such as biosensors and microarrays.

1. Introduction

The precise and stable immobilization of biological macromolecules such as proteins, peptides, nucleic acids, and carbohydrates on solid substrates is a fundamental requirement for the development of modern biosensors, diagnostic platforms, and advanced biomaterials. Creating well-defined biointerfaces is critical for achieving high performance, yet anchoring these sensitive biomolecules while preserving their native function, minimizing non-specific binding, and controlling surface density and orientation remains a major challenge. Traditional methods, including physical adsorption or random covalent coupling, often result in low efficiency, poor specificity, and loss of biological activity due to denaturation. To overcome these limitations, highly specific and efficient bioconjugation strategies are needed. One powerful approach is click chemistry, a concept introduced in 2001 by K. Barry Sharpless and colleagues to describe a class of reactions that are modular, high-yielding, selective, and compatible with mild, aqueous, and environmentally benign conditions. These reactions avoid complex purification steps, rely on readily available reagents, and generate minimal byproducts. With their rapid reaction rates, high specificity, and low toxicity, click chemistry reactions are particularly well suited for chemical biology and biomedical applications, where controlled molecular conjugation is essential [1–13].

Over the past two decades, click chemistry has revolutionized

* Corresponding authors at: Institute of Nanotechnology (INT) & Karlsruhe Nano Micro Facility (KNMFi), Karlsruhe Institute of Technology (KIT), Kaiserstraße 12, 76131 Karlsruhe, Germany; Institute of Nanoscale and Biobased Materials, Faculty of Materials Science and Technology, TU Bergakademie Freiberg, Gustav-Zeuner-Str. 3 09599 Freiberg, Germany.
E-mail addresses: Mahdi.Dadfar@esm.tu-freiberg.de (S.M.M. Dadfar), michael.hirtz@kit.edu (M. Hirtz).

https://doi.org/10.1016/j.surfin.2026.110387
Received 17 March 2026; Received in revised form 28 July 2026; Accepted 11 August 2026
Available online 12 August 2026

multiple fields. In chemical biology, it has become indispensable for bioconjugation of proteins, nucleic acids, and polymers. In medicinal chemistry, it accelerates drug discovery, lead optimization, and imaging probe development. In materials science, it enables the creation of advanced biomaterials, nanotherapeutics, functional surfaces, and well-defined polymers. Its bioorthogonality and robustness even allow in situ and in vivo labelling, diagnostics, and therapeutic applications [5, 14–21].

Click chemistry reactions have revolutionized surface functionalization of glass and other solid substrates by enabling efficient, selective, and bioorthogonal covalent attachment of biomolecules, polymers, and diverse functional groups under mild conditions. This methodology allows for the creation of highly controlled and modular biointerfaces, where the immobilization of antibodies, DNA, peptides, or cells can be achieved with precise orientation and minimal non-specific binding, crucial attributes for high-performance biosensing and diagnostic platforms. The rapid and highly efficient nature of click chemistry enables the dense and stable immobilization of recognition elements on glass and related substrates. By promoting high surface coverage and robust molecular attachment, this strategy enhances the sensitivity, specificity, and reproducibility of biosensing platforms [17–19,22–28]. Recent research has continued to expand the applications of click chemistry for surface functionalization. For example, Dadfar et al. (2018) demonstrated site-specific glass functionalization using azide–alkyne and thiol–alkyne reactions to fabricate high-density molecular microarrays for biomedical assays [29]. In 2019, the same group developed a fluorescent immunosensor for detecting the cancer biomarker AFP by combining multiple click reactions, including thiol–yne, thiol-ene Michael addition (TEMA), strain-promoted azide–alkyne cycloaddition (SPAAC), and ring-opening with a biotin-streptavidin-biotin assembly and antibody-antigen interactions on differently functionalized glass surfaces [30]. Moreover, Klein et al. (2021) reported efficient covalent functionalization of ultrasmall gold nanoparticles via azidation and CuAAC, offering a robust platform for nanoscale biosensors and targeted therapy [31]. Additionally, McGuire et al. (2023) introduced supramolecular click chemistry methods to modify nanoparticle surfaces, enabling tailored bioactive coatings and enhanced biocompatibility [32]. Furthermore, Bukharina et al. (2024) applied copper-free click chemistry to functionalize cellulose nanocrystals with DNA strands, enabling precise nanostructure assembly with tailored optical properties [33]. More recently, Dadfar et al. (2025) extended their work to diamond substrates, comparing different click reactions (TEMA, SPAAC, thiol-yne, and ring-opening) to identify the most efficient strategy for surface functionalization [34].

Among the various reactions that meet the criteria of efficiency and selectivity, the CuAAC, independently reported in 2002 by Sharpless and Meldal, has emerged as the “gold standard.” This reaction enables the rapid and regioselective formation of 1,2,3-triazoles from azides and terminal alkynes, offering exceptional efficiency, high functional group tolerance, and excellent compatibility with biological systems [35,36]. Another powerful approach is the TYC, a fast and efficient process in which thiols add to alkynes under radical initiation (e.g., UV light) to form dithioether products. Unlike the thiol-ene reaction, each alkyne can react with two thiols, enabling the generation of highly functionalized, branched polymers and surfaces particularly suited for advanced materials and biomedical applications [37–39]. This work presents a comprehensive study comparing CuAAC and TYC (Fig. 1) for the surface immobilization of biotin, which serves as a binding site for the biological macromolecule streptavidin. Glass substrates were functionalized with either a small, rigid alkyne (4-pentynoic acid) or a large, flexible alkyne (ALK-PEG-Si). The biotin was patterned onto these surfaces using microchannel cantilever spotting (μCS), and the kinetic progress of the immobilization was monitored at 10, 20, and 40 min. The overall scheme of glass functionalization and subsequent click reactions is illustrated in Fig. 2. The successful binding of biotin was quantified via the subsequent binding of fluorescently labeled streptavidin, a protein macromolecule known for its strong affinity to biotin. This approach allows for a direct correlation between the surface chemistry, the reaction kinetics, and the resulting immobilization of a key biological macromolecule. The findings provide valuable mechanistic insights for the rational design of functional biointerfaces for advanced biomedical and biological applications.

2. Materials and methods

2.1. Materials

All chemicals were used as received without further purification. The key materials are listed in Table 1, including their commercial and short names, roles in the experiment, and sources.

2.2. Preparation of alkyne-terminated glasses via esterification and silanization

2.2.1. Esterification method

Standard glass coverslips (1 × 1 cm, VWR, Germany) were sequentially cleaned with chloroform, 2-propanol, and deionized water, then dried under a nitrogen stream. To generate hydroxyl groups on the glass surface, the coverslips were treated with oxygen plasma (10 sccm O_2, 0.2 mbar, 100 W) for 2 min. A solution containing 4-pentynoic acid (0.02 mmol, 1.96 mg), N,N′-dicyclohexylcarbodiimide (DCC, 0.022 mmol, 4.53 mg), and 4-dimethylaminopyridine (DMAP, 0.0035 mmol, 0.43 mg) was prepared in DMSO. The hydroxyl-functionalized glass substrates were immersed in this solution and incubated at room temperature for 24 h under a nitrogen atmosphere to allow esterification. After the reaction, the samples were washed twice with DMSO (5 min each), twice with ethanol (5 min each), rinsed with deionized water, and finally dried under a nitrogen stream.

2.2.2. Silanization method

For the silanization approach, the cleaned and plasma-activated glass coverslips were immersed in a 2% w/v solution of alkyne-PEG-silane (MW ~3400 Da) prepared in a 95:5 ethanol:water mixture. The reaction was carried out at room temperature for 5 h. Afterwards, the samples were washed sequentially with ethanol, acetone, and deionized water, then dried under a nitrogen stream.

2.3. Characterization of the surface by X-ray photoelectron spectroscopy (XPS)

XPS measurements were performed on a K-Alpha+ spectrometer (Thermo Fisher Scientific, East Grinstead, UK). The Thermo Avantage software was used for data acquisition and processing. A monochromated Al Kα X-ray source with a 400 μm spot size was used for all measurements. Photoelectrons were analyzed with a 180° hemispherical analyzer operated in constant analyzer energy mode at a pass energy of

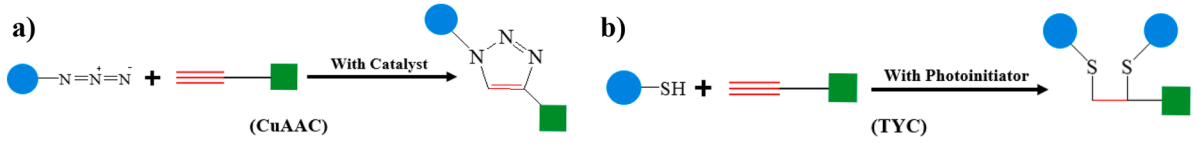

Fig. 1. Schematic representation of the two click reactions used in this study: (a) (CuAAC) and (b) (TYC) reaction.

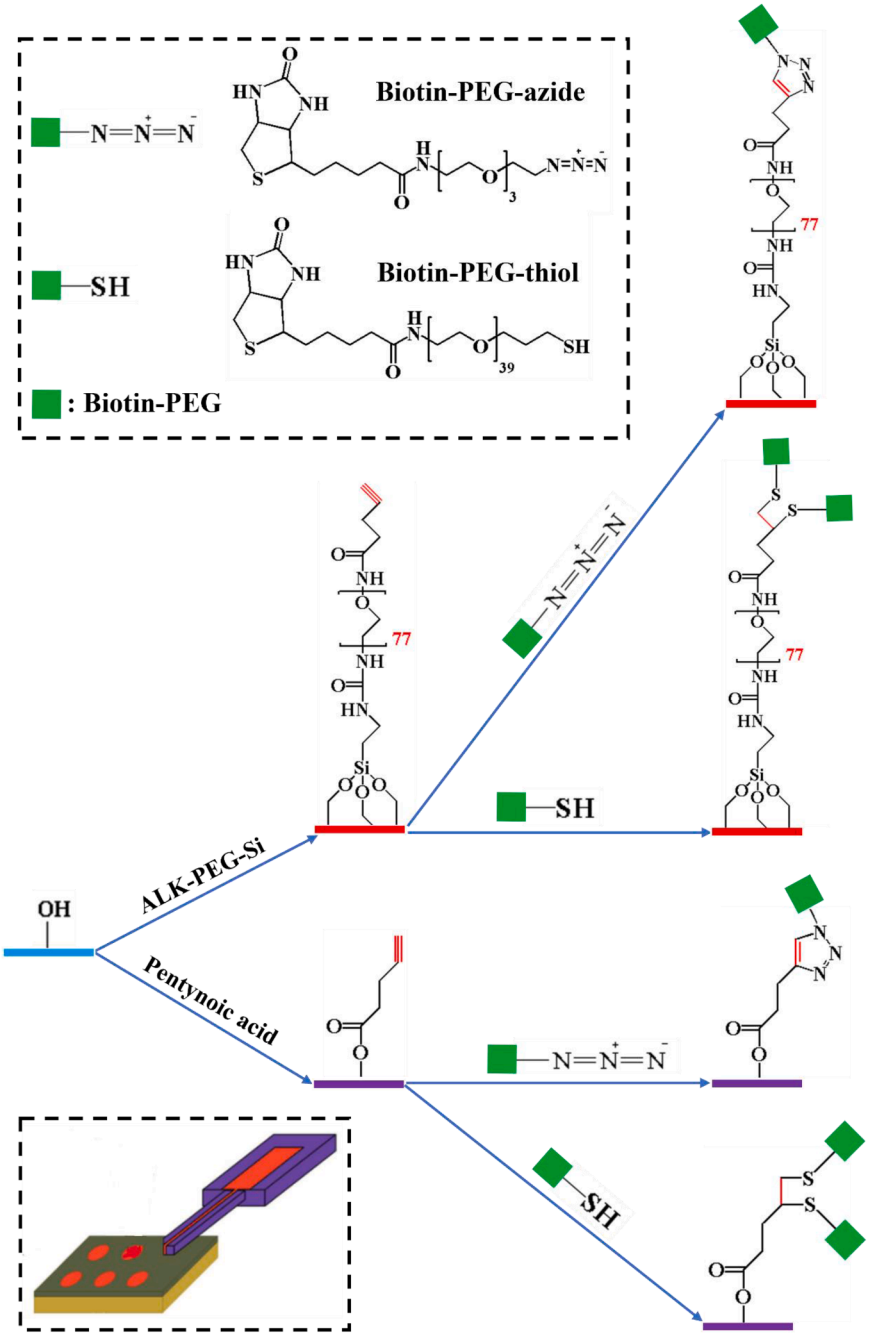

Fig. 2. Schematic representation of glass surface functionalization and subsequent click reactions.

Table 1
List of chemicals used in this work.

Commercial name	Short name	Role	Source
4-Pentynoic acid	Pentynoic acid	coupling agent in esterification	Sigma-Aldrich (Germany)
Alkyne PEG Silane	ALK-PEG-Si	coupling agent in silanization	Nanocs Company (USA)
Streptavidin-Cy3	Streptavidin	Conjugation with biotinylated molecules	Sigma-Aldrich (Germany)
Azide-PEG_3-biotin conjugate, MW=500	Biotin-azide	Nonfluorescent dye (biotinylated molecule)	Jena Bioscience (Germany)
Biotin PEG Thiol, MW=2000	Biotin-thiol	Nonfluorescent dye (biotinylated molecule)	Nanocs Company (USA)
4-Dimethylaminopyridine	DMAP	Photoinitiator	Sigma-Aldrich (Germany)
Sodium ascorbate	Na-ascorbate	Reduction reagent	Jena Bioscience (Germany)
Copper(II)-Sulphate	$CuSO_4$	Catalyst	Jena Bioscience (Germany)
N,N′-dicyclohexylcarbodiimide	DCC	Catalyst	Sigma-Aldrich (Germany)
Bovine serum albumin	BSA	Blocker	Sigma-Aldrich (Germany)
Phosphate buffer saline	PBS	Buffer	Sigma-Aldrich (Germany)
Dimethyl sulfoxide	DMSO	Solvent	Sigma-Aldrich (Germany)
Glycerol	-	-	Sigma-Aldrich (Germany)

50 eV for high-resolution elemental spectra. Charge compensation was achieved using the K-Alpha+ system with 8 eV electrons and low-energy argon ions to minimize local charging. Spectral fitting was performed using Voigt line shapes (binding energy uncertainty ± 0.2 eV), and quantitative analysis employed Scofield sensitivity factors [40]. All spectra were calibrated to the C 1 s hydrocarbon peak (C-C/C-H) at 285.0 eV, with accuracy further verified against reference metallic Cu, Ag, and Au photoelectron peaks.

2.4. Surface roughness analysis via atomic force microscopy (AFM)

Surface roughness was characterized using Atomic Force Microscopy (AFM) on a Dimension Icon system (Bruker, Germany) operating in tapping mode with HQ:NSC15/Al BS cantilevers (MikroMasch, USA). Measurements were conducted in air under ambient conditions using the NanoScope 8.10 software. Roughness was quantified as the root-mean-square (RMS) deviation of surface height (denoted as Rq), extracted from 5 × 5 μm^2 scan areas. For each sample, four different surface regions were analyzed, and the average RMS roughness was calculated to ensure representative values.

2.5. Water contact angle measurements

The static contact angles of water droplets on both bare and functionalized glass surfaces were measured at room temperature using an OCA-20 contact angle analyzer (DataPhysics Instruments GmbH, Germany). For each sample, five water droplets (2 μL each) were dispensed at a consistent rate of 2 μL s^{-1} onto different regions of the surface. The average contact angle from these measurements was calculated and reported.

2.6. Ink solution preparation

The dyes used for the μCS were biotin-azide for the CuAAC reaction and biotin thiol for the TYC click reaction, both performed on alkyne-terminated glass. For the biotin-azide ink, the solutions consisted of 5 μL $CuSO_4$ (10 mM in DI water), 5 μL sodium ascorbate (20 mM in DI water), and 1 μL biotin-azide (500 μg mL^{-1} in DMSO) was prepared. For the biotin-thiol ink, a biotin-thiol solution (200 μg mL^{-1} in DMSO) was prepared, to which DMPA (2 mol% relative to biotin-thiol) was added as a photoinitiator. Both inks were finally mixed with glycerol in a 7:3 (ink: glycerol) ratio.

2.7. Pattern writing via μCS for click chemistry reactions

Patterning was carried out using the NLP 2000 system (NanoInk, USA) equipped with SPT pens (SPT-S-C10S, Bioforce Nanosciences). Prior to use, the pen was cleaned with oxygen plasma (10 sccm O_2, 0.2 mbar, 100 W, 2 min) and used immediately. The pen reservoir was loaded with 0.2 μL of the ink solution. Spotting was performed at a controlled relative humidity of 20%, with a dwell time of 2 s for all patterns. After printing the biotin-azide ink, samples were left at room temperature for 10, 20, or 40 min before washing. For the biotin-thiol ink, printed samples were irradiated using a 365 nm UV LED source positioned approximately 20 cm above the substrate, corresponding to an irradiation intensity of approximately 10 mW cm^{-2}, for 10, 20, or 40 min, followed by washing.

2.8. Protein binding on microarrays

The binding of fluorescently labeled streptavidin to arrays of two distinct biotin-conjugates immobilized on functionalized glass via click reactions was investigated. Prior to streptavidin incubation, the samples were blocked with 10% bovine serum albumin (BSA) in PBS for 30 minutes to minimize nonspecific binding around the microarrays. Subsequently, the samples were washed three times by pipetting 30 μL of PBS on and off the surface. They were then incubated for 1 hour with a 10 μg·mL^{-1} streptavidin solution in the dark. After incubation, the samples were washed three more times with PBS, rinsed with deionized water, and dried using a gentle stream of nitrogen before fluorescence microscopy analysis.

2.9. Fluorescence microscopy technique

Fluorescence imaging was performed using a Nikon Eclipse 80i upright fluorescence microscope (Nikon, Japan), equipped with Intensilight illumination (Nikon, Japan), a CoolSNAP HQ2 camera (Photometrics, USA), and a Texas Red filter (λabs = 559 nm, λem = 630 nm, color-coded red). Image acquisition and analysis were carried out using NIS-Elements software (Nikon, Japan). The average fluorescence intensity per feature was quantified, and the resulting data were tabulated for diagram preparation and statistical analysis.

2.10. Statistical analysis

All data were expressed as the means plus standard deviations. The significant differences between treatments were analyzed using one-way ANOVA and Duncan tests ($P < 0.05$) with the statistical package for the social sciences (SPSS, version 19.0.0 Abacus Concepts, Berkeley, California, USA).

3. Result and discussion

3.1. XPS measurement

XPS results confirmed the successful stepwise functionalization of hydroxyl-terminated glass via both ALK-PEG-Si and pentynoic acid routes followed by click conjugation with biotin derivatives (Fig. 3). For the ALK-PEG-Si pathway (Fig. 3A and B), the C 1 s spectrum of bare glass showed mainly adventitious C–C/C–H (~285.0 eV), while silanization (b) introduced a pronounced C–O/C–N component (~286.4 eV), consistent with PEG chains. Subsequent click reactions with biotin azide (c) and biotin thiol (d) bring additional N–C=O contribution at 288.3 eV characteristic of biotin amide groups and increased overall carbon intensity (from ~ 5 at% for the bare glass up to ~25 at% for the functionalized glass surfaces), indicating successful conjugation. The N 1 s spectra corroborated these findings, showing an increase in nitrogen content (up to ~3 at%) and the appearance of peaks at 400.2 eV (amide N–C=O) and 402.0 eV (protonated or triazole N^+), confirming azide-alkyne cycloaddition and biotin immobilization. Similar trends were observed for the pentynoic acid route (Fig. 3C and D), even if the first step of functionalization could not be clearly proven since the attached molecule is very small. Nevertheless, the C 1 s spectrum shows the appearance of the N-C=O component at 288.3 eV after click reactions (c, d) indicating the attachment of PEG-biotin conjugates. Progressive increases in N 1 s intensity from ~0.3 (surface contamination) up to ~3.0 at% across the modification steps, along with the presence of amide and triazole nitrogen species, confirm efficient surface coupling. It should be noted that given the length of the PEG chain of the biotin thiol, a higher contribution of the C-O component could be expected. This can be explained by a very probable smaller density of attachment of this bigger molecule on the small pentynoic molecule because of steric hindrance. Overall, the combined C 1 s and N 1 s analyses verify the formation of PEG-rich organic layers and successful click-mediated biotin functionalization for both surface modification strategies.

3.2. AFM analysis

In this study, AFM was employed to evaluate the topographical and roughness changes of glass surfaces after sequential functionalization and biotin conjugation (Figs. 4 and 5). Bare glass exhibited the lowest surface roughness (~0.25 nm), consistent with a clean, unmodified

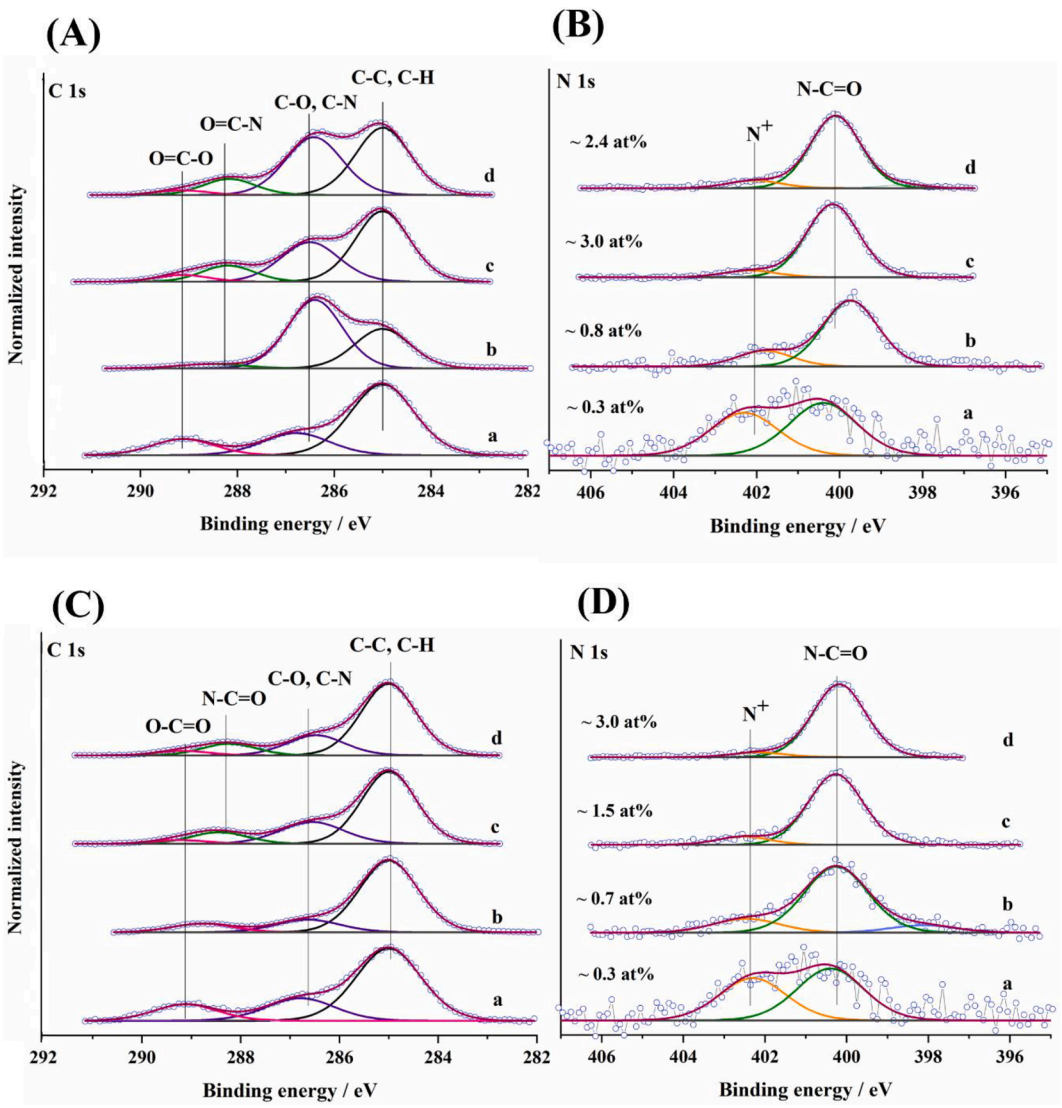

Fig. 3. XPS analysis of stepwise surface functionalization and click conjugation on glass substrates. High-resolution C 1 s (A, C) and N 1 s (B, D) spectra showing the chemical evolution of hydroxyl-terminated glass after modification and biotin coupling. (A–B) Functionalization via ALK-PEG-Si: (a) OH-terminated glass, (b) PEG-silane layer, (c) click reaction with biotin azide, and (d) click reaction with biotin thiol. (C–D) Functionalization via pentynoic acid: (a) OH-terminated glass, (b) pentynoic acid layer, (c) click reaction with biotin azide, and (d) click reaction with biotin thiol.

substrate (Fig. 5a). Functionalization with pentynoic acid or ALK-PEG-Si resulted in a modest increase in roughness, indicating successful monolayer formation (Fig. 5b and e). The slightly higher roughness observed for the PEG-silane surface compared to pentynoic acid reflects the greater steric bulk and conformational flexibility of the PEG linker [41,42].

Click conjugation with biotin azide induced the largest roughness increases for both alkyne-modified surfaces, as visually demonstrated by the dense nanostructured clusters appearing in the 3D surface profiles (Fig. 5c and f). This pronounced effect is attributed to the CuAAC, which incorporates bulky biotin moieties using a markedly short PEG_3 spacer. The short length and structural rigidity of this 3-unit PEG chain limit its freedom of conformational rotation, forcing the bulky biotin molecules into close lateral proximity. This restriction leads to heightened molecular crowding, steric hindrance, and subsequent localized surface clustering or partial multi-layer aggregation. In contrast, biotin thiol conjugation produced a moderate increase in surface roughness. This smaller change suggests that thiol attachment, possibly via thiol-surface interactions or disulfide formation, generates more ordered and less clustered surface architectures compared to the azide–alkyne click reaction [43], a behavior strongly governed by the structural characteristics of its highly elongated PEG_{39} spacer arm. The much longer 39-unit PEG chain possesses substantial conformational flexibility, allowing the chains to bend or coil more horizontally along the functionalized silane matrix. This flexibility effectively cushions and dissipates the steric bulk of the biotin headgroups, distributing them across a larger spatial regime to generate a more homogeneous, less clustered surface architecture as structurally evident in the smoother topography of the control surfaces (Fig. 5d and g).

Statistical analysis supports these trends: as shown in Fig. 4, there is a significant difference in roughness for the biotin azide conjugation samples, which are rougher than all other groups, while the biotin thiol conjugation samples show a significant but smaller increase compared to unmodified and single-functionalized surfaces.

These findings align with previous AFM studies, where PEG-silane or carboxylic acid-functionalized glass surfaces show moderate roughness increases upon monolayer formation, and CuAAC-based biotin attachment leads to substantial roughness enhancements due to bulky group incorporation [42,43]. In this work, the largest roughness changes were observed for biotin azide click reactions, particularly with the

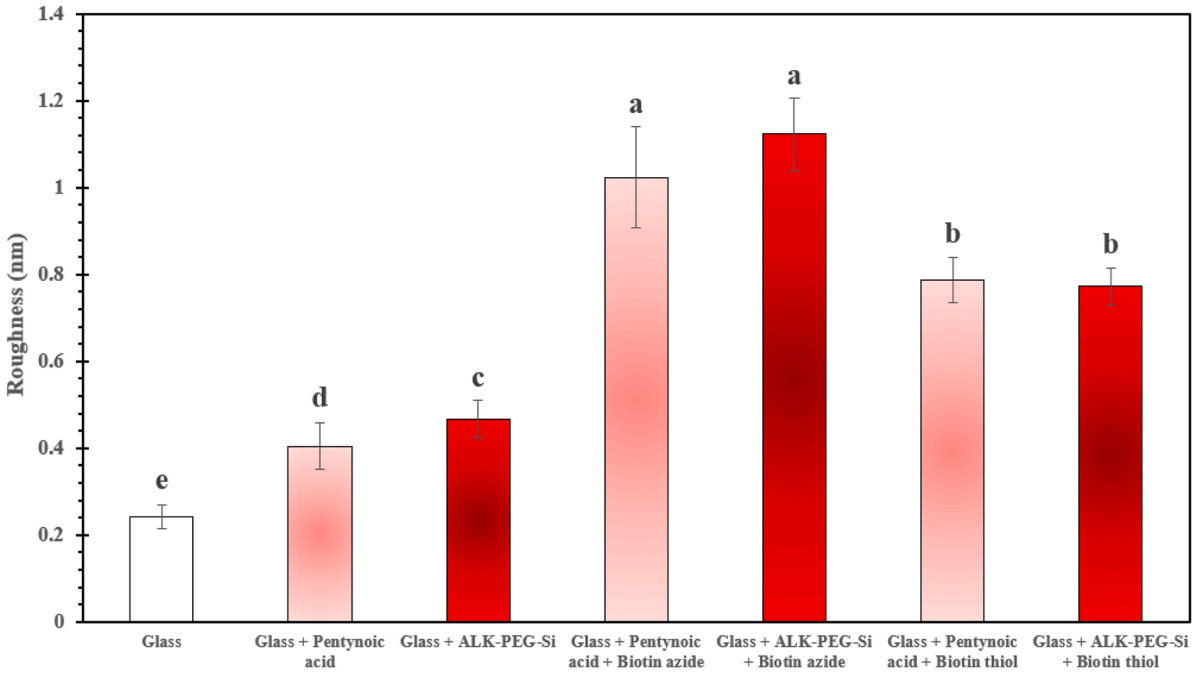

Fig. 4. Roughness of glass surfaces after successive functionalization and click reaction steps, as measured by atomic force microscopy (AFM). Different letters (a-e) indicate statistically significant differences between the groups ($p < 0.05$).

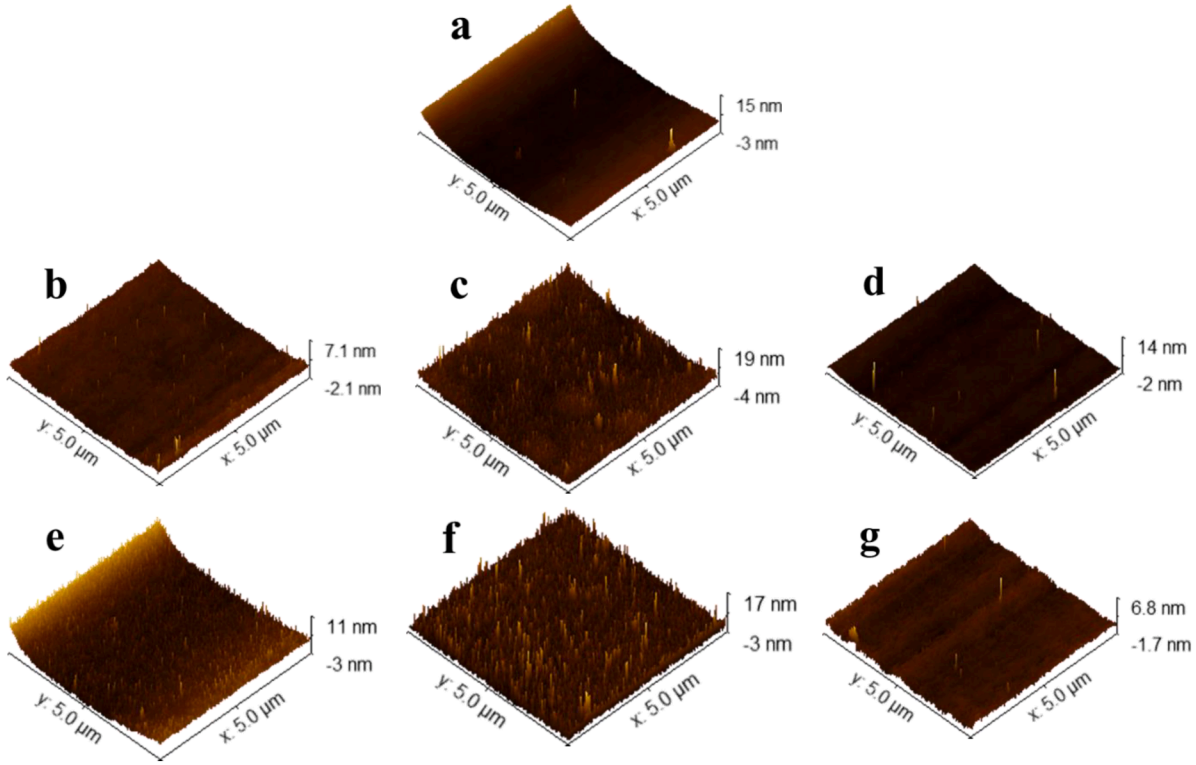

Fig. 5. 3D AFM images (5.0 µM × 5.0 µM) for glass (a), glass + Pentynoic acid (b), glass + Pentynoic acid + Biotin azide (c), glass + Pentynoic acid + Biotin thiol (d), glass + ALK-PEG-Si (e), glass + ALK-PEG-Si (f), and glass + ALK-PEG-Si (g).

ALK-PEG-Si linker, confirming efficient and dense surface modification. Biotin thiol conjugation yielded milder roughness changes, consistent with a more ordered attachment mechanism.

3.3. Contact angle measurement

The success and stability of the surface functionalization were quantitatively evaluated using water contact angle goniometry, with measurements taken over a 21-day period to assess the dynamic changes in wettability (Fig. 6). Following plasma treatment, glass surfaces

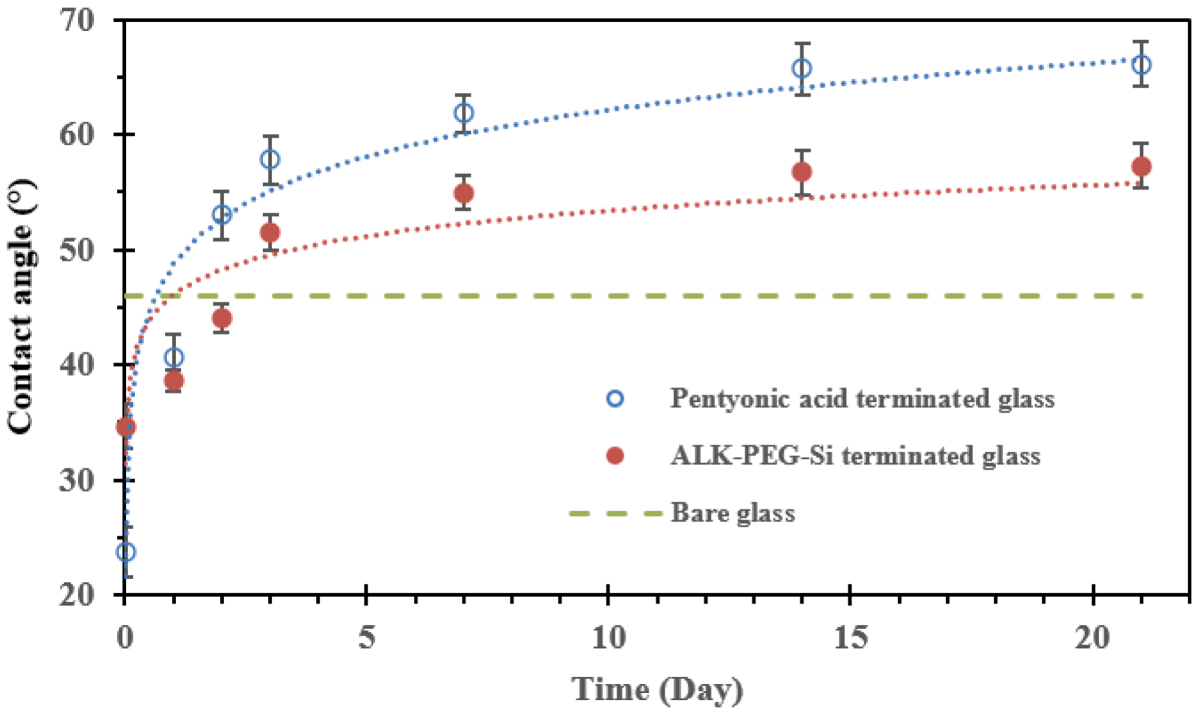

Fig. 6. Contact angle of water droplets as a function of time on bare glass, pentynoic acid terminated glass, and ALK-PEG-Si terminated glass.

exhibited an initial contact angle near zero, consistent with a highly hydrophilic, hydroxyl-rich surface. This extreme wettability aligns with prior reports that plasma exposure dramatically increases OH group density, rendering glass superhydrophilic, though such states are inherently unstable and subject to hydrophobic recovery over time [24,29,44].

Upon functionalization, distinct differences in long-term wettability emerged when comparing pentynoic acid and ALK-PEG-Si modifications against bare glass. Unmodified glass surfaces stabilized at a contact angle of ~46°, corresponding to the moderate, stable hydrophilicity of native silanol and siloxane groups. Glass modified with pentynoic acid displayed a pronounced increase, reaching ~66° after 21 days. This indicates successful esterification and formation of a hydrophobic alkyl monolayer, with initial lower values likely attributable to residual plasma-induced hydroxyls that diminish over time. As these unstable groups recover or are replaced, the pentynoic acid coating imparts robust hydrophobicity, consistent with prior studies of alkyl chain functionalization [45,46].

In contrast, silanization with ALK-PEG-Si (77 PEG units) produced a stable contact angle of ~57° throughout the measurement period. The PEG linker conferred moderate hydrophilicity, lower than that of pentynoic acid, due to its ethylene glycol repeat units. The initial low value, followed by gradual stabilization, reflects the loss of unreacted plasma-induced hydroxyl groups and maturation of the PEG-silane monolayer, in line with previously reported aging profiles for PEG-modified glass [42,47].

Overall, the time-dependent evolution of water contact angle demonstrates the dynamic interplay of plasma treatment, chemical functionalization, and monolayer stability. Pentynoic acid terminated glass achieves higher hydrophobicity due to alkyl chain coverage, while PEG modification yields a more hydrophilic yet stable wettability profile. These findings confirm successful surface engineering and are consistent with established literature on glass modification, wettability, and surface aging effects [47,48]. The distinct wettability profiles of the two surfaces thus create different microenvironments that directly influence the kinetics and efficiency of macromolecular immobilization, as detailed in the following sections.

3.4. Comparative analysis of streptavidin immobilization via CuAAC and TYC

The efficiency of streptavidin immobilization on alkyne-functionalized glass surfaces was evaluated using two click-chemistry strategies: CuAAC with biotin azide and TYC with biotin thiol. Glass substrates functionalized with either pentynoic acid or ALK-PEG-Si (PEG77) were reacted with biotin azide or biotin thiol for 10, 20, or 40 min. Following the click reactions, the substrates were thoroughly rinsed with deionized water to remove residual catalyst, unreacted biotin molecules, and loosely adsorbed species. The modified surfaces were then incubated with fluorescent streptavidin to allow binding to the immobilized biotin groups. After incubation, the substrates were washed to remove unbound streptavidin, and the fluorescence intensity was subsequently measured to quantify protein immobilization. Kinetic analysis revealed that streptavidin binding after CuAAC-mediated biotin immobilization was strongly influenced by the underlying surface chemistry (Fig. 7). Quantitative fluorescence analysis revealed that at 10 min, both pentynoic acid and ALK-PEG-Si surfaces displayed comparably low intensities, consistent with limited biotin immobilization during short incubation. At 20 min, however, ALK-PEG-Si exhibited nearly twice the fluorescence intensity of pentynoic acid, indicating that the flexible PEG linker facilitates more efficient conjugation at intermediate times. By 40 min, fluorescence intensities increased further and converged between the two surface chemistries, demonstrating that prolonged CuAAC reactions reach similarly high coupling efficiencies regardless of the linker. Statistical analysis confirmed these trends, with ALK-PEG-Si showing significantly higher signals than pentynoic acid at 20 min, while no significant differences were detected at 10 or 40 min. The images in Fig. 7 show only selected portions of the 15 × 15 spot arrays and are intended for qualitative visualization. Quantitative fluorescence values in Fig. 8 were calculated by averaging measurements from 30 spots distributed across different regions of each array to account for potential local variations.

The fluorescence signal was attributed to specific biotin-streptavidin interactions. It should be noted that nonspecific adsorption of fluorescent streptavidin on alkyne-terminated surfaces was previously

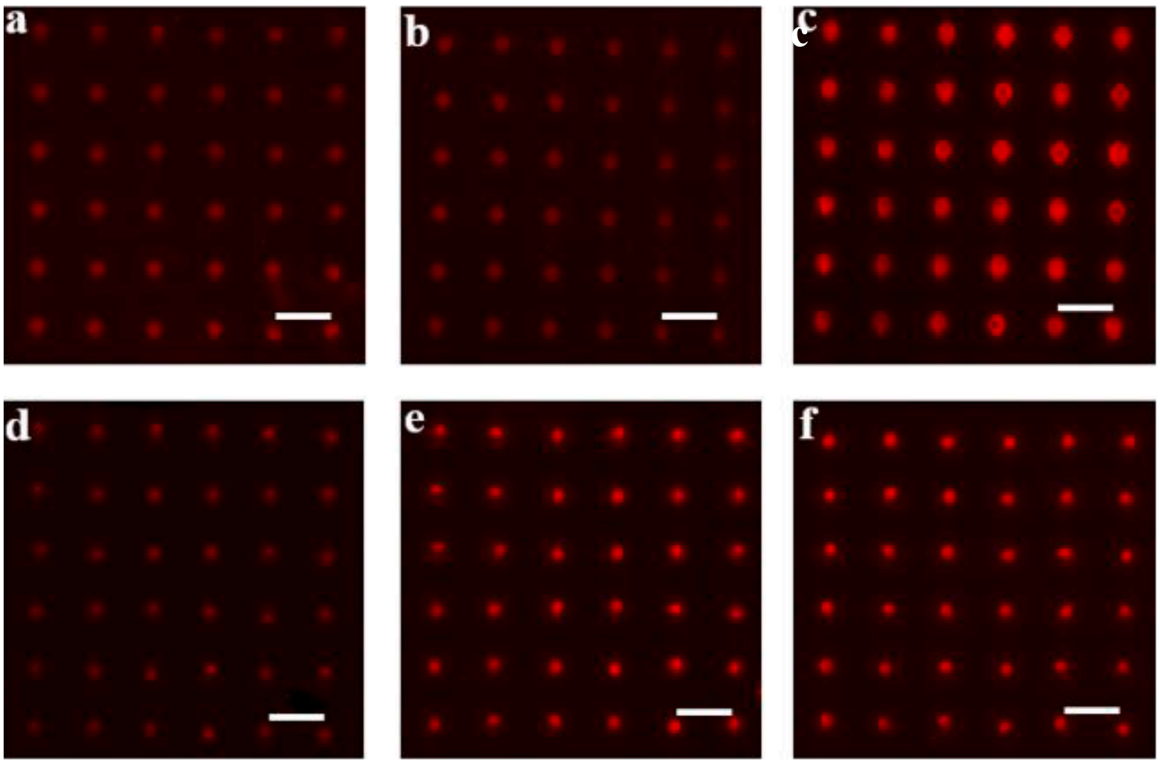

Fig. 7. Representative fluorescence microarray images of CuAAC bound biotin after streptavidin-Cy3 binding. Glass substrates were functionalized with either pentynoic acid (a–c) or Alkyne PEG silane (d–f) and subsequently reacted with μCS spotted biotin azide for 10 min (a,d), 20 min (b,e), or 40 min (c,f). The patterned biotin azide was visualized by subsequently incubating Cy3 labelled streptavidin. Scale bars equal 50 μm.

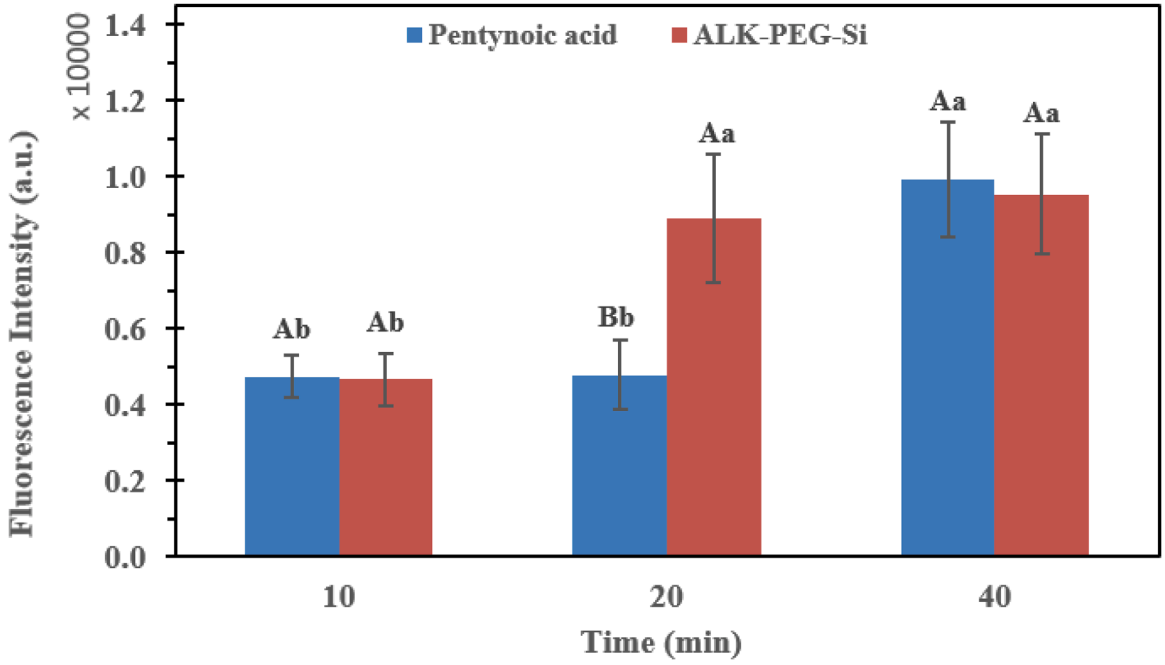

Fig. 8. Fluorescence intensity analysis of microarray biotin azide immobilization via CuAAC on pentynoic acid vs. ALK-PEG-Si functionalized substrates. For the same alkyne group, values with different lowercase letters indicate significant differences across different times; for the same time point, values with different uppercase letters indicate significant differences between the two alkyne groups ($p < 0.05$, according to Duncan's multiple range test).

investigated under identical experimental conditions. No residual fluorescence was observed after the rinsing step, whereas biotin-functionalized surfaces retained strong fluorescence, confirming that the measured signal originates from specific biotin-streptavidin binding rather than nonspecific protein adsorption [34]. Therefore, the fluorescence intensities reported here can be directly correlated with the efficiency of biotin immobilization achieved through the respective click reactions. It should also be noted that the fluorescence measurements were used to quantify the amount of immobilized streptavidin and, consequently, the efficiency of biotin immobilization. The present study

did not directly evaluate the retention of the native biotin-binding activity of the immobilized streptavidin, which would require a dedicated functional binding assay.

These kinetic differences can be explained by the distinct chemical environments created by the two linkers. PEG linkers generate a hydrated, flexible, and anti-fouling surface that enhances the accessibility of terminal alkyne groups for CuAAC. The extended PEG chains reduce non-specific adsorption and steric hindrance, thereby allowing biotin azide to couple more efficiently [42,43]. As a result, PEGylated surfaces achieve higher immobilization densities and yield stronger fluorescence signals. The anti-fouling properties of PEG also support greater surface coverage by biotin azide, further amplifying the observed differences in fluorescence intensity [42,49].

In contrast, short-chain alkynes such as pentynoic acid present a more rigid, hydrophobic, and crowded interface. The limited chain mobility and closer molecular packing reduce the accessibility of surface alkyne groups, restricting biotin azide coupling and leading to lower fluorescence intensities [49]. The hydrophobic character of pentynoic acid surfaces may further diminish protein–surface interactions, reducing immobilization efficiency compared to PEGylated surfaces. Taken together, these findings are consistent with well-documented trends showing that PEGylation promotes more efficient and specific biomolecule immobilization, while small-molecule linkers are more prone to crowding effects and reduced reactivity [42,49,50]. Thus, the superior performance of ALK-PEG-Si in CuAAC immobilization is rooted in its ability to present accessible and reactive alkyne groups within a hydrated, anti-fouling environment.

The kinetic profile of the TYC reaction presented a stark contrast to that of CuAAC (Fig. 9). Quantitative fluorescence values shown in Fig. 10 revealed that at 10 min, pentynoic acid surfaces displayed substantially higher fluorescence than ALK-PEG-Si surfaces, suggesting that the shorter linear linker permits faster radical addition, while steric shielding within the PEG brush delays efficient reaction. At 20 min, fluorescence increased for both surfaces, with pentynoic acid still producing stronger signals, although the difference was reduced. By 40 min, fluorescence intensities on both surface types converged, indicating that extended UV irradiation allows radicals to penetrate the PEG layer and react with available alkyne groups. Statistical analysis confirmed these trends, showing that pentynoic acid significantly outperformed ALK-PEG-Si at 10 min, while no significant differences remained at 40 min [22]. The faster initial reactivity of pentynoic acid can be attributed to its short, rigid structure, which leaves terminal alkyne groups fully exposed at the glass interface. With minimal steric hindrance, biotin thiol rapidly accesses and reacts with surface alkynes, producing strong fluorescence intensities during early irradiation. This direct accessibility gives pentynoic acid a distinct kinetic advantage in the short term. By contrast, ALK-PEG-Si surfaces, while more hydrated and conformationally flexible, present a sterically bulkier environment that initially limits thiol accessibility [42,49]. The dense PEG layer can act as a barrier, slowing the diffusion of biotin thiol and reducing early radical addition rates. However, as UV irradiation continues, PEG chains undergo dynamic conformational rearrangements, gradually exposing additional reactive alkyne groups. This process reduces the initial kinetic barrier and allows PEGylated surfaces to “catch up” over time [22,42].

With prolonged irradiation, PEG linkers provide further advantages. Their hydration shell and anti-fouling properties minimize non-specific adsorption and progressively support higher biotin densities as more thiol molecules diffuse to the surface. Ultimately, this enables ALK-PEG-Si to achieve fluorescence intensities comparable to those of pentynoic acid, despite its slower start. At equilibrium, PEGylated surfaces offer not only efficient immobilization but also cleaner, more specific coverage than shorter hydrophobic linkers [42,49].

Taken together, these observations align with published studies on TYC click chemistry, which consistently report that short-chain alkynes favor faster initial thiol addition due to direct accessibility, while PEGylated surfaces reach similar or higher immobilization levels after extended irradiation, owing to their dynamic flexibility and anti-fouling

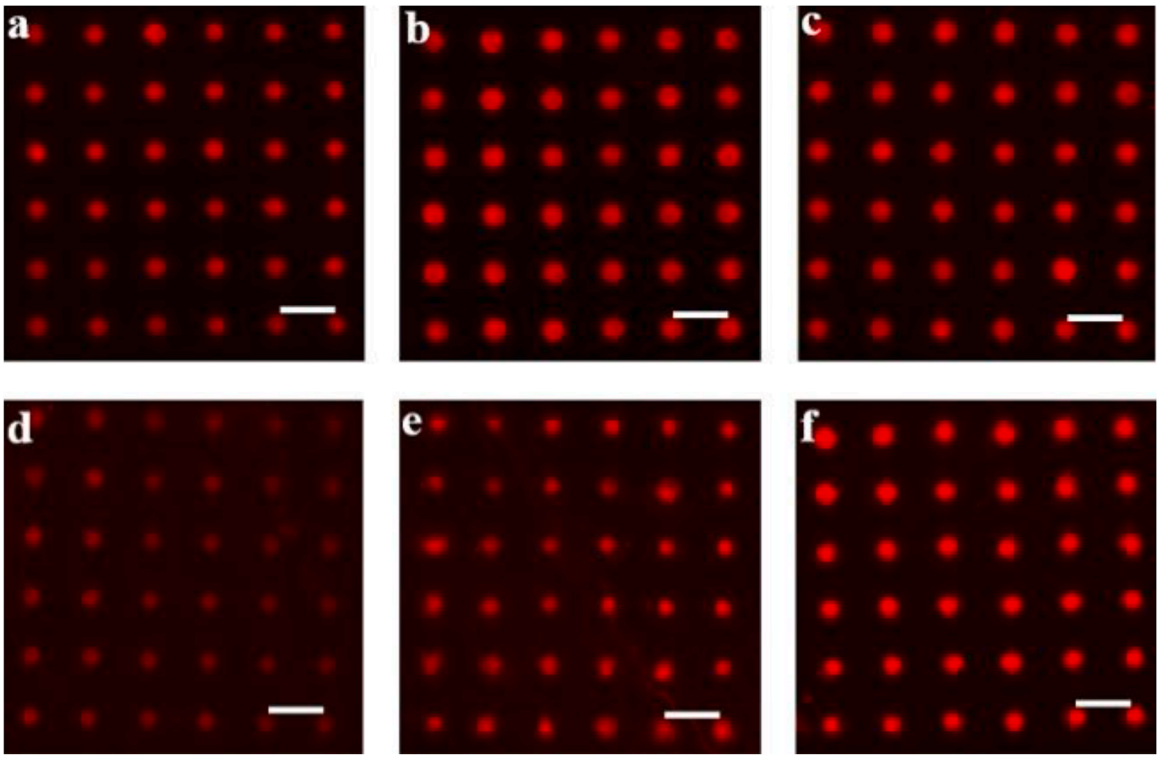

Fig. 9. Representative fluorescence microarray images of TYC bound biotin after streptavidin-Cy3 binding. Glass substrates were functionalized with either pentynoic acid (a–c) or ALK-PEG-Si (d–f) and subsequently reacted with μCS spotted biotin thiol for 10 min (a,d), 20 min (b,e), or 40 min (c,f) Patterned biotin thiol was visualized by binding streptavidin labelled with Cy3 dye. Scale bars equal 50 μm.

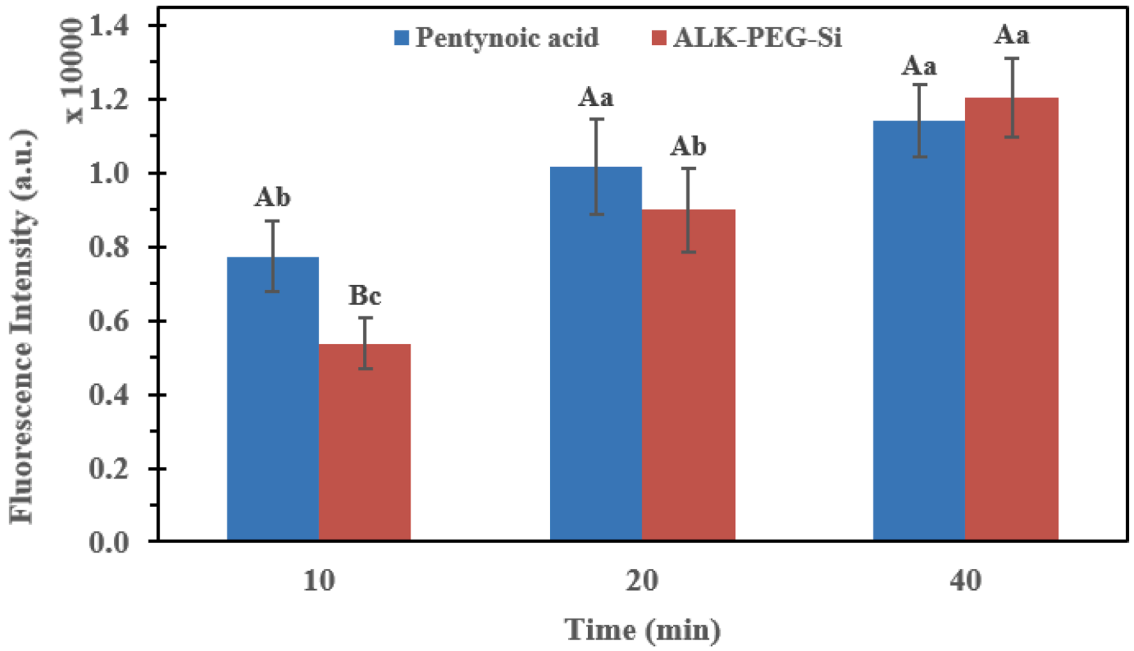

Fig. 10. Fluorescence intensity analysis of microarray biotin thiol immobilization via TYC on pentynoic acid vs. ALK-PEG-Si functionalized substrates. For the same alkyne group, values with different lowercase letters indicate significant differences across different times; for the same time point, values with different uppercase letters indicate significant differences between the two alkyne groups ($p < 0.05$, according to Duncan's multiple range test).

behavior. Thus, both surface chemistries are compatible with biotin thiol immobilization: pentynoic acid excels in short-term kinetics, whereas ALK-PEG-Si offers comparable long-term efficiency along with superior control over non-specific binding.

To provide a clear overview of how surface chemistry and linker choice influence wettability, roughness, and the kinetics of biotin immobilization via CuAAC and TYC, the key parameters are summarized in Table 2. This table highlights the differential performance of pentynoic acid and ALK-PEG-Si surfaces, showing that PEGylated surfaces favor high-density, anti-fouling immobilization via CuAAC, while pentynoic acid promotes faster initial TYC kinetics. By consolidating contact angle, surface roughness, and reaction intensity data, Table 2 offers a concise comparison of overall performance for each functionalization strategy and provides context for the kinetic trends discussed above.

A comparison of the two click strategies highlights clear differences in kinetics and surface dependence. CuAAC enabled rapid and efficient biotin immobilization, particularly on ALK-PEG-Si, where the hydrated and flexible linker enhanced alkyne accessibility and minimized non-specific adsorption. Pentynoic acid surfaces showed slower coupling, but after 40 min both surfaces reached similarly high immobilization. In contrast, TYC proceeded more slowly overall and was strongly influenced by surface architecture. Pentynoic acid supported faster attachment at short irradiation times due to readily accessible alkynes, while ALK-PEG-Si initially lagged because of steric shielding. However, with prolonged UV exposure, PEG chains rearranged to expose additional reactive groups, allowing both surfaces to converge to comparable immobilization levels.

Taken together, the results demonstrate that the relative performance of CuAAC and TYC depends strongly on the surface architecture and reaction conditions. CuAAC generally provided higher immobilization efficiencies on PEGylated surfaces, whereas TYC exhibited faster initial kinetics on pentynoic acid-functionalized surfaces and offers the additional advantage of being a metal-free click reaction. Both chemistries ultimately achieved effective biotin immobilization and streptavidin attachment after prolonged reaction times.

3.5. *Synthesis and broader implications for biological macromolecular engineering*

A comparative analysis of the two click chemistries highlights that the choice of linker is not arbitrary; it is a critical design parameter that dictates the optimal reaction strategy for a given application. The data presented here demonstrate that PEG linkers favor the CuAAC reaction, which provides a high-density, anti-fouling platform ideal for sensitive applications like protein microarrays where a clean background is crucial. The CuAAC reaction on the PEG surface offers a balance of efficient binding kinetics and a protein-friendly environment.

Conversely, the short, rigid 4-pentynoic acid linker is particularly suitable for TYC, a metal-free click reaction that enables exceptionally fast initial kinetics. This strategy is advantageous for applications that require rapid surface functionalization, such as point-of-care diagnostics or rapid prototyping of biomaterial surfaces. At longer time points, both

Table 2
Summary of surface and kinetic properties for each functionalization strategy.

Surface Chemistry	Wettability (Contact Angle)	Surface Roughness (RMS)	Initial CuAAC Kinetics (10 min)	Final CuAAC Intensity (40 min)	Initial TYC Kinetics (10 min)	Final TYC Intensity (40 min)	Overall Performance Summary
4-pentynoic acid	Moderately hydrophobic (~66°)	Low/Moderate	Slow	High	Fast	High	Favors rapid kinetics via TYC; less suitable for CuAAC
ALK-PEG-Si	Moderately hydrophilic (~57°)	Moderate	Slow/Moderate	Very High	Fast	Very High	Favors high-density, anti-fouling surfaces for both chemistries; superior for CuAAC

CuAAC and TYC, regardless of the linker, achieve similarly high levels of biotin and, by extension, streptavidin immobilization. This finding offers a degree of flexibility in choosing the optimal strategy based on the time constraints and specific requirements of the application.

The observed differences in surface roughness and wettability directly correlate with the performance of the immobilized streptavidin macromolecule. The smoother, more hydrophilic PEG surface facilitates better protein binding and reduces non-specific background, which is a critical metric for biosensor performance. This underscores the importance of a holistic approach to biomaterial design, where the initial surface chemistry and the final macromolecular assembly are seen as a single, integrated system.

Overall, the present results indicate that the choice between CuAAC and TYC should be guided by the desired balance between immobilization efficiency, reaction kinetics, surface architecture, and catalyst requirements rather than by the assumption that one click chemistry is universally superior.

4. Conclusion

This study provides a comprehensive comparative analysis of CuAAC and TYC click chemistries for the immobilization of biological macromolecules on two distinct alkyne-functionalized glass surfaces. While both chemistries and both surfaces ultimately resulted in similar high-density streptavidin immobilization after 40 min, their kinetic profiles and underlying mechanisms were fundamentally different. CuAAC was more efficient on the flexible and hydrophilic PEG-based surface, which provided a mobile, hydrated, and anti-fouling environment that promoted rapid and specific coupling. In contrast, TYC was significantly faster on the rigid, short-chain alkyne surface, where the direct accessibility of the reactive groups enabled rapid radical-initiated coupling. The findings underscore that the selection of both the linker chemistry and the click reaction type is a crucial design decision for optimizing the fabrication of microscale patterns for biological applications. For applications demanding rapid patterning and short reaction times, TYC with a short-chain linker is the superior strategy. For applications requiring high-density, low-background protein microarrays and long-term stability, CuAAC with a flexible PEG linker is the optimal choice. This work offers a practical guide and a deeper mechanistic understanding for researchers to tailor the properties of biomaterial interfaces for specific biological and biomedical needs, ultimately advancing the field of macromolecular engineering and functional biointerface design.

Declaration of generative AI and AI-assisted technologies in the writing process

During the preparation of this work, the authors used OpenAI's tool ChatGPT to enhance the readability, clarity, and fluency of the text. After using this tool, the authors reviewed and edited the content as needed and took full responsibility for the content of the publication.

CRediT authorship contribution statement

Seyed Mohammad Mahdi Dadfar: Writing – original draft, Methodology, Investigation, Formal analysis, Data curation, Conceptualization, Writing – review & editing. **Sylwia Sekula-Neuner:** Writing – review & editing, Conceptualization, Methodology. **Vanessa Trouillet:** Formal analysis, Data curation, Investigation, Writing – original draft, Writing – review & editing. **Yvonne Joseph:** Writing – review & editing, Resources. **Michael Hirtz:** Supervision, Project administration, Funding acquisition, Conceptualization, Resources, Writing – review & editing.

Declaration of competing interest

The authors declare that they have no known competing financial interests or personal relationships that could have appeared to influence the work reported in this paper.

Acknowledgements

This work was partly carried out with the support of the Karlsruhe Nano Micro Facility (KNMF, https://www.knmf.kit.edu), a Helmholtz Research Infrastructure at Karlsruhe Institute of Technology (KIT, https://www.kit.edu). S.M.M.D. and M.H. gratefully acknowledge support by the Deutsche Forschungsgemeinschaft (DFG) under grant HI 1724/3-1. S.M.M.D. acknowledges support by the German Academic Exchange Service (DAAD) and the Karlsruhe House of Young Scientists (KHYS) in the form of a STIBET grant.

Data availability

No data was used for the research described in the article.

References

[1] Z. Geng, J.J. Shin, Y. Xi, C.J. Hawker, Click chemistry strategies for the accelerated synthesis of functional macromolecules, J. Polym. Sci. 59 (2021) 963–1042, https://doi.org/10.1002/pol.20210126.
[2] H.C. Kolb, M.G. Finn, K.B. Sharpless, Click chemistry: diverse chemical function from a few good reactions, Angew. Chem., Int. Ed. 40 (2001) 2004–2021, https://doi.org/10.1002/1521-3773(20010601)40:11<2004::AID-ANIE2004>3.0.CO;2-5.
[3] M.S. Singh, S. Chowdhury, S. Koley, Advances of azide-alkyne cycloaddition-click chemistry over the recent decade, Tetrahedron 72 (2016) 5257–5283, https://doi.org/10.1016/j.tet.2016.07.044.
[4] P. Thirumurugan, D. Matosiuk, K. Jozwiak, Click chemistry for drug development and diverse chemical–biology applications, Chem. Rev. 113 (2013) 4905–4979, https://doi.org/10.1021/cr200409f.
[5] J. Kaur, M. Saxena, N. Rishi, An overview of recent advances in biomedical applications of click chemistry, Bioconjug. Chem. 32 (2021) 1455–1471, https://doi.org/10.1021/acs.bioconjchem.1c00247.
[6] A. Pasieka, E. Diamanti, E. Uliassi, M.Laura Bolognesi, Click chemistry and targeted degradation: a winning combination for medicinal chemists? ChemMedChem. 18 (2023) e202300422 https://doi.org/10.1002/cmdc.202300422.
[7] S.L. Scinto, D.A. Bilodeau, R. Hincapie, W. Lee, S.S. Nguyen, M. Xu, C.W. am Ende, M.G. Finn, K. Lang, Q. Lin, Bioorthogonal chemistry, Nat. Rev. Method. Primer. 121 (2021) 6991–7031, https://doi.org/10.1021/acs.chemrev.0c00799.
[8] J. Hu, W. Wang, B. Zhou, J. Sun, W.S. Chin, L. Lu, Click chemistry in lithium-metal batteries, Small. 20 (2024) 2306622, https://doi.org/10.1002/smll.202306622.
[9] F. Rusmini, Z. Zhong, J. Feijen, Protein immobilization strategies for protein biochips, Biomacromolecules 8 (2007) 1775–1789, https://doi.org/10.1021/bm061197b.
[10] P. Jonkheijm, D. Weinrich, H. Schröder, C.M. Niemeyer, H. Waldmann, Chemical strategies for generating protein biochips, Angew. Chem., Int. Ed. 47 (2008) 9618–9647, https://doi.org/10.1002/anie.200801711.
[11] K. Nakanishi, T. Sakiyama, K. Imamura, On the adsorption of proteins on solid surfaces, a common but very complicated phenomenon, J. Biosci. Bioeng. 91 (2001) 233–244, https://doi.org/10.1016/S1389-1723(01)80127-4.
[12] K.E. Sekhosana, S.A. Majeed, U. Feleni, Click chemistry in the electrochemical systems: toward the architecture of electrochemical (bio) sensors, Coord. Chem. Rev. 491 (2023) 215232, https://doi.org/10.1016/j.ccr.2023.215232.
[13] K. Song, Y. Liu, Q. Ma, C. Liang, L. Mao, Y. Jiang, Electrochemical tyrosine-click bioconjugation enables multiplexed cytokine sensing and immunoprofiling in native serum, Nat. Commun. 17 (2026), https://doi.org/10.1038/s41467-026-70815-3.
[14] M.M.A. Mitry, F. Greco, H.M.I. Osborn, In vivo applications of bioorthogonal reactions: chemistry and targeting mechanisms, Chem.–A Eur. J. 29 (2023) e202203942, https://doi.org/10.1002/chem.202203942.
[15] C.D. Hein, X.-M. Liu, D. Wang, Click chemistry, a powerful tool for pharmaceutical sciences, Pharm. Res. 25 (2008) 2216–2230, https://doi.org/10.1007/s11095-008-9616-1.
[16] R. Zhao, J. Zhu, X. Jiang, R. Bai, Click chemistry-aided drug discovery: a retrospective and prospective outlook, Eur. J. Med. Chem. 264 (2024) 116037, https://doi.org/10.1016/j.ejmech.2023.116037.
[17] N.K. Devaraj, M.G. Finn, Introduction: click chemistry, ACS Publicat. 121 (2021) 6697–6698, https://doi.org/10.1021/acs.chemrev.1c00469.
[18] S. Bhatia, A. Biharee, S. Mondal, S. Kulkarni, R. Kumar, S. Thareja, Mechanistic analysis of diverse click reactions along with their applications, Eur. J. Med. Chem. 296 (2025) 117800, https://doi.org/10.1016/j.ejmech.2025.117800.
[19] T. Luu, K. Gristwood, J.C. Knight, M. Jorg, Click chemistry: reaction rates and their suitability for biomedical applications, Bioconjug. Chem. 35 (2024) 715–731, https://doi.org/10.1021/acs.bioconjchem.4c00084.
[20] S. Asad, D. Ahl, Y.C. Del Suárez-López, M. Erdélyi, M. Phillipson, A. Teleki, Click chemistry-based bioconjugation of iron oxide nanoparticles, Small 21 (2025) 2407883, https://doi.org/10.1002/smll.202407883.

[21] N.Z. Fantoni, A.H. El-Sagheer, T. Brown, A hitchhiker's guide to click-chemistry with nucleic acids, Chem. Rev. 121 (2021) 7122–7154, https://doi.org/10.1021/acs.chemrev.0c00928.
[22] A.B. Lowe, Thiol-ene "click" reactions and recent applications in polymer and materials synthesis, Polym. Chem. 1 (2010) 17–36, https://doi.org/10.1039/b9py00216b.
[23] S.M.M. Dadfar, S. Sekula-Neuner, V. Trouillet, M. Hirtz, Protein microarray immobilization via epoxide ring-opening by thiol, amine, and azide, Adv. Mater. Interface. 8 (2021) 2002117, https://doi.org/10.1002/admi.202002117.
[24] S.M.M. Dadfar, S. Sekula-Neuner, V. Trouillet, M. Hirtz, A comparative study of thiol-terminated surface modification by click reactions: thiol-yne coupling versus thiol-ene Michael addition, Adv. Mater. Interface. 5 (2018) 1801343, https://doi.org/10.1002/admi.201801343.
[25] B. Yang, K. Gordiyenko, A. Schäfer, S.M.M. Dadfar, W. Yang, K. Riehemann, R. Kumar, C.M. Niemeyer, M. Hirtz, Fluorescence imaging study of film coating structure and composition effects on DNA hybridization, Adv. Nanobiomed. Res. 3 (2023) 2200133, https://doi.org/10.1002/anbr.202200133.
[26] Y. Tu, Y. Yang, Y. Zheng, S. Guo, J. Shen, Polyvinylidene fluoride based piezoelectric composites with strong interfacial adhesion via click chemistry for self-powered flexible sensors, Small 20 (2024) 2309758, https://doi.org/10.1002/smll.202309758.
[27] Z. Zhang, T. Li, Y. Sheng, L. Liu, H.-C. Wu, Enhanced sensitivity in nanopore sensing of cancer biomarkers in human blood via click chemistry, Small 15 (2019) 1804078, https://doi.org/10.1002/smll.201804078.
[28] F. Wang, Y. Xie, W. Zhu, T. Wei, Recent advances in functionalization strategies for biosensor interfaces, especially the emerging electro-click: a review, Chemosensors 11 (2023) 481, https://doi.org/10.3390/chemosensors11090481.
[29] S.M.M. Dadfar, S. Sekula-Neuner, U. Bog, V. Trouillet, M. Hirtz, Site-specific surface functionalization via microchannel cantilever spotting (μCS): comparison between Azide–Alkyne and Thiol–Alkyne click chemistry reactions, Small 14 (2018) 1800131, https://doi.org/10.1002/smll.201800131.
[30] S.M.M. Dadfar, S. Sekula-Neuner, V. Trouillet, H.-Y. Liu, R. Kumar, A.K. Powell, M. Hirtz, Evaluation of click chemistry microarrays for immunosensing of alpha-fetoprotein (AFP), Beilst. J. Nanotechnol. 10 (2019) 2505–2515, https://doi.org/10.3762/bjnano.10.241.
[31] K. Klein, K. Loza, M. Heggen, M. Epple, An efficient method for covalent surface functionalization of ultrasmall metallic nanoparticles by surface azidation followed by copper-catalyzed azide-alkyne cycloaddition (click chemistry), ChemNanoMat. 7 (2021) 1330–1339, https://doi.org/10.1002/cnma.202100359.
[32] K. McGuire, S. He, J. Gracie, C. Bryson, D. Zheng, A.W. Clark, J. Koehnke, D. J. France, W.M. Nau, T.-C. Lee, Supramolecular click chemistry for surface modification of quantum dots mediated by cucurbit [7]uril, ACS Nano 17 (2023) 21585–21594, https://doi.org/10.1021/acsnano.3c06601.
[33] D. Bukharina, K. Cauffiel, L.M. Killingsworth, J.A. Brackenridge, V. Poliukhova, M. Kim, J. Brower, J. Bernal-Chanchavac, N. Stephanopoulos, V.V. Tsukruk, Click-chemistry-enabled functionalization of cellulose nanocrystals with single-stranded DNA for directed assembly, ACS Biomater. Sci. Eng. 10 (2024) 6155–6166, https://doi.org/10.1021/acsbiomaterials.4c01518.
[34] S.M.M. Dadfar, S. Sekula-Neuner, M. Hirtz, Enhancing diamond biosensors and photonic devices: the interplay of surface roughness, functionalization, and fluorescence, Adv. Mater. Interface. 12 (2025) e00378, https://doi.org/10.1002/admi.202500378.
[35] S.S. Ragab, Signature of click chemistry in advanced techniques for cancer therapeutics, RSC Adv. 15 (2025) 10583–10601, https://doi.org/10.1039/d5ra01196e.
[36] V.V. Rostovtsev, L.G. Green, V.V. Fokin, K.B. Sharpless, A stepwise huisgen cycloaddition process: copper (I)-catalyzed regioselective" ligation" of azides and terminal alkynes, Angew. Chem., Int. Ed. 41 (2002) 2596–2599, https://doi.org/10.1002/1521-3773(20020715)41:14<2596::AID-ANIE2596>3.0.CO;2-4.
[37] L. George, A. Varghese, Advancements in thiol-yne click chemistry: recent trends and applications in polymer synthesis and functionalization, Mater. Today Chem. 38 (2024) 102112, https://doi.org/10.1016/j.mtchem.2024.102112.
[38] B. Yao, J. Sun, A. Qin, B.Z. Tang, Thiol-yne click polymerization, Chin. Sci. Bull. 58 (2013) 2711–2718, https://doi.org/10.1007/s11434-013-5892-1.
[39] S. Lü, Z. Wang, S. Zhu, Thiol-yne click chemistry of acetylene-enabled macrocyclization, Nat. Commun. 13 (2022) 5001, https://doi.org/10.1038/s41467-022-32723-0.
[40] J.H. Scofield, Hartree-Slater subshell photoionization cross-sections at 1254 and 1487 eV, J. Electron. Spectros. Relat. Phenomena 8 (1976) 129–137, https://doi.org/10.1016/0368-2048(76)80015-1.
[41] R.A. Jaikumar, S. Karthigeyan, T.R. Bhat, M. Naidu, G.P. Raj, S. Natarajan, Analysis of surface roughness and three-dimensional scanning topography of zirconia implants before and after photofunctionalization by atomic force microscopy: an In vitro study, J. Pharm. Bioall. Sci. 13 (2021) S766–S771, https://doi.org/10.4103/jpbs.JPBS_724_20.
[42] S. Jo, K. Park, Surface modification using silanated poly (ethylene glycol) s, Biomaterials 21 (2000) 605–616, https://doi.org/10.1016/S0142-9612(99)00224-0.
[43] Y. Gidi, S. Bayram, C.J. Ablenas, A.S. Blum, G. Cosa, Efficient one-step PEG-silane passivation of glass surfaces for single-molecule fluorescence studies, ACS Appl. Mater. Interface. 10 (2018) 39505–39511, https://doi.org/10.1021/acsami.8b15796.
[44] J.I. Mendez-Linan, E. Ortiz-Ortega, M.F. Jimenez-Moreno, M.I. Mendivil-Palma, E. Martínez-Guerra, F.S. Aguirre-Tostado, S.O. Martinez-Chapa, S. Hosseini, M. J. Madou, Aging effect of plasma-treated carbon surfaces: an overlooked phenomenon, Carbon N. Y. 169 (2020) 32–44, https://doi.org/10.1016/j.carbon.2020.06.085.
[45] T. Vukovic, J. Røstad, U. Farooq, O. Torsæter, A. van der Net, Systematic study of wettability alteration of glass surfaces by dichlorooctamethyltetrasiloxane silanization- A guide for contact angle modification, ACS Omega 8 (2023) 36662–36676, https://doi.org/10.1021/acsomega.3c02448.
[46] A. Rosenfeld, M. Brehm, A. Welle, V. Trouillet, S. Heissler, M. Benz, P.A. Levkin, Solid-phase combinatorial synthesis using microarrays of microcompartments with light-induced on-chip cell screening, Mater. Today Bio 3 (2019) 100022, https://doi.org/10.1016/j.mtbio.2019.100022.
[47] S. Watson, C. Pattyn, M. Mohseni Garakani, A. Ajji, S. Reuter, M.R. Wertheimer, Wetting and aging behaviors for several O2 and NH3 plasma treated nanofibrous and flat film polymer materials: a comparison, Plasm. Process. Polym. 20 (2023) e2200224, https://doi.org/10.1002/ppap.202200224.
[48] T. Egghe, R. Ghobeira, R. Morent, R. Hoogenboom, N. de Geyter, Comparative study of the aging behavior of plasma activated hexamethyldisiloxane-based plasma polymers and silicone elastomer thin films, Prog. Org. Coat. 172 (2022) 107091, https://doi.org/10.1016/j.porgcoat.2022.107091.
[49] Y.S. Lin, V. Hlady, C.-G. Gölander, The surface density gradient of grafted poly (ethylene glycol): preparation, characterization and protein adsorption, Colloid. Surf., B 3 (1994) 49–62, https://doi.org/10.1016/0927-7765(93)01114-7.
[50] M.J.E. Fischer, Amine coupling through EDC/NHS: a practical approach. Surface Plasmon resonance: Methods and Protocols, Springer, 2010, pp. 55–73, https://doi.org/10.1007/978-1-60761-670-2_3.